Thermochemical properties, electronic structure and bonding of mixed lithium boron clusters (BnLi, n = 1 −8) and their anions

ARTICLE *in* CHEMICAL PHYSICS · JULY 2010

Impact Factor: 1.65 · DOI: 10.1016/j.chemphys.2010.07.015

2 AUTHORS:

Truong Tai
University of Leuven
65 PUBLICATIONS **506** CITATIONS

SEE PROFILE

Minh Tho Nguyen
University of Leuven
748 PUBLICATIONS **10,835** CITATIONS

SEE PROFILE

Chemical Physics 375 (2010) 35–45

Contents lists available at ScienceDirect

Chemical Physics

journal homepage: www.elsevier.com/locate/chemphys

Thermochemical properties, electronic structure and bonding of mixed lithium boron clusters (B_nLi, n = 1–8) and their anions

Truong Ba Tai [a], Minh Tho Nguyen [a,b,*]

[a] Department of Chemistry, LMCC-Mathematical Modeling and Computational Science Center, Katholieke Universiteit Leuven, B-3001 Leuven, Belgium
[b] Institute for Computational Science and Technology of HoChiMinh City, Viet Nam

ARTICLE INFO

Article history:
Received 18 May 2010
In final form 13 July 2010
Available online 17 July 2010

Keywords:
Boron clusters
Mixed lithium boron clusters
Ab initio calculations
Heats of formation
Normalized resonance energy

ABSTRACT

The electronic structure and molecular properties of a series of small mixed lithium boron clusters B_nLi (n = 1–8) in both neutral and anionic states are investigated using quantum chemical methods. The lowest-energy structures are identified. Standard heats of formation, adiabatic electron affinities (EAs) and vertical detachment energies (VDEs) are predicted using coupled-cluster theory CCSD(T)/6-311+G(d) calculations. Addition of Li to B_n to form B_nLi clusters marginally distorts the geometries of the parent B_n. The chemical bond in B_nLi has a highly ionic character in which the positive charges are located on Li. MO analysis confirms a similar degree of aromaticity between B_nLi and B_n^-. The relative stabilities of the clusters are evaluated using the average binding energy (E_b), second order difference in energy (Δ^2E), resonance energy (RE) and normalized resonance energy (NRE). Both REs and NREs quantities of the Li-doped boron clusters are consistently larger than those of the pure B_n clusters. The B_3Li species exhibits a remarkably high stability within the B_nLi series.

1. Introduction

The boron clusters continue to attract much attention of theoretical and experimental scientists alike due to their interesting physical and chemical properties. During the past decades, a large number of investigations have been reported on the global minima, chemical bonding nature [1–9], spectroscopic properties [10–15] and thermochemical parameters [16–18] of the small bare boron clusters B_n (n = 2–20) in the neutral, cationic and anionic states. It was pointed out that these small boron clusters strongly prefer a planar shape [6,10,11] and the three-dimensional geometries become favored only from the clusters containing more than 20 atoms. Furthermore, most of the small bare boron clusters can be considered as σ-aromatic, π-aromatic or doubly (π and σ) aromatic species, that are in line with their high stability and planarity [6,10,11,17–20].

Mixed clusters containing boron and lithium are even more intriguing. The lithium element is usually a good electron donor and tends to form chemical bonding with highly ionic nature. For instance, the chemical bonding, and in particular the aromaticity of the mixed clusters containing boron and alkali and alkaline earth metals were also investigated by Li and co-workers [21–23], including the series of $M@B_5$ (M = Li, Na, K, Rb, Cs), $M@B_5^+$ (M = Be, Mg, Ca, Sr), $M@B_6$ (M = Be, Mg, Ca, and Sr), and also LiB_7 and BeB_7^+. The structures of the boron rings have been analyzed in detail. Spectroscopic parameters of LiB_n (n = 6, 8) determined by Alexandrova et al. [24,25] suggested that these mixed clusters exhibit a highly ionic character in their chemical bonds.

Recently, we reinvestigated the electronic structure, thermochemical parameters and growth mechanisms of the small B_n clusters, their monoxides and dioxides, B_nO_m, with n = 1–13 and m = 1–2, together with their anions [16–18]. To evaluate the molecular stability, we employed the resonance energy (RE) index, that was defined earlier by Dewar and deLlano [26a] and recently updated by Dixon and co-workers [26b]. In addition, we defined the normalized resonance energy (NRE), which is a simple index to quantify the cluster stability [18]. The most typical feature of B_nO_m species is the strength of the BO bond. As a consequence, a stable structure of a neutral boron monoxide is obtained by either condensing O on a BB edge of a B_n cycle, or binding one BO group to a B_{n-1} ring. This becomes a dominant feature in the boron dioxides. The BO group mainly behaves as an electron-withdrawing substituent reducing the binding energy and resonance energy of the oxides. Overall, the latter conserve the planarity and multiple aromaticity of the parent boron clusters [18]. Considering oxygen as an electronegative element, the effects of lithium, which is a

* Corresponding author at: Department of Chemistry, LMCC-Mathematical Modeling and Computational Science Center, Katholieke Universiteit Leuven, B-3001 Leuven, Belgium.
E-mail address: minh.nguyen@chem.kuleuven.be (M.T. Nguyen).

0301-0104/$ - see front matter © 2010 Elsevier B.V. All rights reserved.
doi:10.1016/j.chemphys.2010.07.015

strongly electropositive element, on the clusters are of considerable interest.

Although theoretical studies on mixed lithium boron clusters B_nLi were reported for a few sizes, no systematic investigation for this series has been performed to study the effects of the Li doping on boron clusters. In this context, we set out to perform a consistent theoretical prediction of the geometries, thermodynamic stabilities, chemical bonding and aromaticity of the B_nLi clusters with $n = 1–8$, in conjunction with their anions, using quantum chemical methods. These systematic results allow us to gain more insight for chemical bonding and stability feature of small clusters B_nLi. The bonding nature in the series of B_n, B_nO and B_nLi are also compared, as well as the growth mechanism of the B_nLi system is probed.

2. Computational methods

All electronic structure calculations are carried out using the Gaussian 03 [27] and MOLPRO 2006 [28] program packages. Equilibrium geometries and harmonic vibrational frequencies for $n = 1–8$ are fully computed using density functional theory with the hybrid B3LYP functional [29–31] that includes the Becke's three parameter nonlocal exchange functional with the nonlocal correlation functionals of Lee, Yang and Parr. In this work, all the possible isomers of each B_nLi system are initially constructed by doping one Li-atom at all positions of the lower-lying isomers of the pure boron B_n. For example, B_6Li isomers are constructed by doping Li-atom into all the positions of each of the lower-lying B_6 isomers and optimized at the B3LYP/6-31G(d) level. Subsequently, the local minima without imaginary frequencies are reoptimized at a higher level of theory (B3LYP/6-311+G(d)). Where available, the structures are compared with the literature results. Thus, we are confident that the global minima are reached.

For smaller species ($n = 1–5$), geometry optimizations are also performed using the second-order Møller–Plesset perturbation theory (MP2) method [32]. The polarized split-valence plus diffuse functions 6-311+G(d) basis set [33–35], that was found to be effective enough for the LiB_n system [24,25] is used in this set of calculations. Total atomization energies (TAE) are subsequently calculated using the restricted/unrestricted coupled-cluster R/UCCSD(T) formalism [36–39]. By combining the calculated TAE values with the known heats of formation at 0 K for the elements, $\Delta H_f^\circ(B) = 135.1 \pm 0.2$ kcal/mol [40], and $\Delta H_f^\circ(Li) = 37.7$ kcal/mol [41], the ΔH_f° values at 0 K of the B_nLi species can be evaluated. A rationale for the choice of the heat of formation for the boron atom has been given previously [42]. The heats of formation at 298 K are then derived by adding the corresponding thermal corrections [43]. The energetic parameters REs and NREs terms are evaluated using the calculated TAEs and heats of formation. It should be stressed that in our recent studies [16–18] the CCSD(T) energies were calculated using the correlation consistent aug-cc-pVaZ (a = D, T, Q) basis sets, and subsequently extrapolated to the complete basis set limit (CBS). Due to the lack of computational resources, only CCSD(T) calculations with the smaller 6-311+G(d) basis set can be computed in the present work for the whole series of B_nLi clusters. As a consequence, the energetic values obtained here are obviously less accurate for the heats of formation, with an expected error of ±3.0 kcal/mol on the heats of formation (instead of ±1.0 kcal/mol previously achieved with CBS calculations). However, the relative energies between isomers, or the EAs and VDEs, obtained here are found to be closer to the CBS values.

The natural bond orbitals (NBO) [44–46] and the topology of the electron localization function (ELF) [47] are also constructed using B3LYP/6-311+G(d) densities. The ELF plots are supplemented by a determination of their topological bifurcations [48]. The ELF is as a local measure of the Pauli repulsion between electrons owing to the exclusion principle in 3D space. Such a localization technique allows the partition of a total density into basins, which correspond to the molecular regions containing the cores, lone pairs and chemical bonds. The total ELF's are mapped out using the TOPMOD software [49] and all ELF isosurfaces are plotted using the Gopenmol software [50]. The expectation $\langle S^2 \rangle$ values of the UHF wavefunctions, that is a measure of the spin contamination, is given in Table S3 of the ESI.

3. Results and discussion

We first consider the geometries and thermochemical parameters of the B_nLi clusters in both neutral and anionic states. An analysis of their aromatic character and the topology of electron densities, as well as the energetic parameters characterizing the stabilities of clusters, are subsequently presented.

3.1. Molecular structures and thermochemical parameters

The optimized shapes, symmetry point groups, electronic states and relative energies of the B_nLi ($n = 1–8$) clusters considered in both neutral and anionic states are displayed in Figs. 1–6. The neutral clusters having an even number of B are studied in both doublet and quartet electronic states, whereas those with an odd

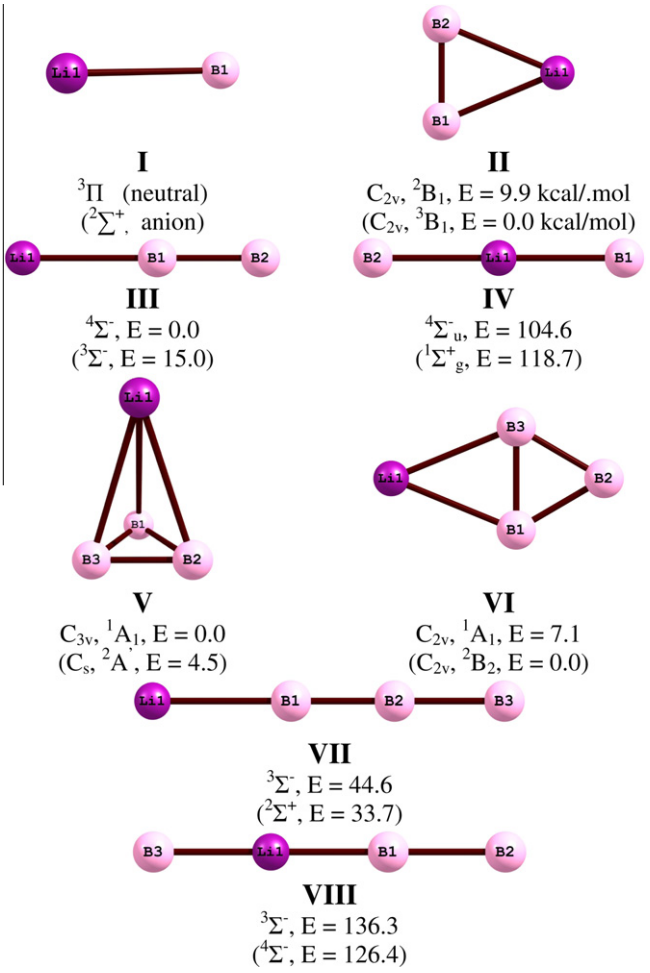

Fig. 1. Shape of the lowest-energy structures B_nLi and B_nLi^- with $n = 1–3$. Relative energies (E) are given in kcal/mol for the neutrals (upper) and anions (lower).

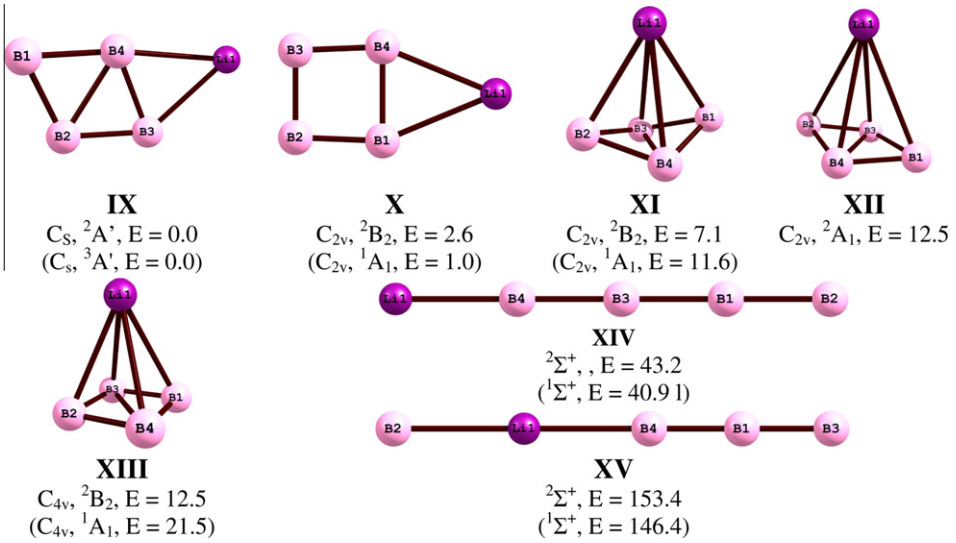

Fig. 2. Shape of the lowest-energy structures B_4Li and their anions. Relative energies (E) are given in kcal/mol for the neutrals (upper) and anions (lower).

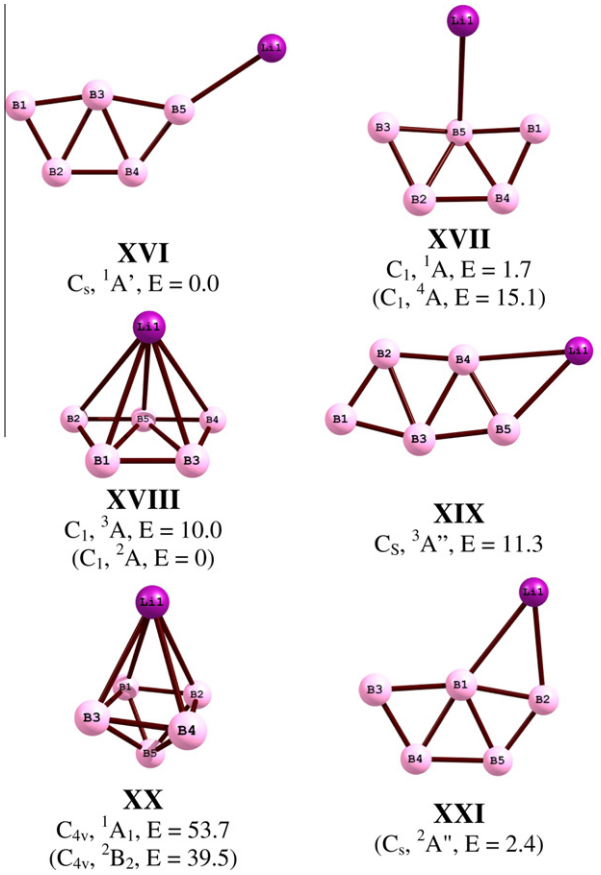

Fig. 3. Shape of the lowest-energy structures B_5Li and their anions. Relative energies (E) are given in kcal/mol for the neutrals (upper) and anions (lower).

number of B are examined in both singlet and triplet states. A reversed situation is considered for the B_nLi^- anions. The total atomization energies (TAE), the heats of formation (ΔH_f) at both 0 and 298 K are given in Table 1. Calculated electron affinities (EAs) of B_nLi and vertical detachment energies (VDEs) of B_nLi^- are shown in Tables 2 and 3, respectively. The charge populations are tabulated in Table 4. For the purpose of comparison, the NICS values of B_nLi and B_n having a closed shell configuration are given in Table 5. To consider the effects of adding one Li-atom into B_n, the electronic energies of global minima for B_n and B_n^- whose geometries were reported in our previous papers [17,18] are recalculated at the CCSD(T)/6-311+G(d)//B3LYP/6-311+G(d) level (the relevant energetic values are summarized in the Supplementary Information). All energetic values given hereafter are obtained using the 6-311+G(d) basis set.

3.1.1. BLi

The high spin $^3\Pi$ state is confirmed to be the ground state of BLi. The lowest-lying excited state is the low spin $^1\Sigma^+$ [51,52] with the corresponding singlet–triplet gap amounting to 5.8 kcal/mol (CCSD(T)). The bond dissociation energy $D_0(^3\Pi)$ is calculated at 24.1 kcal/mol at the same level, that agrees with the values given in previous reports using different methods, namely 26.5 kcal/mol by G2(MP2), 26.6 kcal/mol by QCISD [52] and 27.2 kcal/mol by QCISD(T)/6-311+G(2df)//MP2/6-311+G(d) [53]. The B3LYP/6-311+G(d) bond length of the $^3\Pi$ state is 2.131 Å, that is 0.267 Å shorter than that of the excited state $^1\Sigma^+$ (2.398 Å). Natural population analysis reveals a high ionic character of the neutral BLi($^3\Pi$), with a strongly positive net charge on Li (q(Li) = 0.74 electron). Following such a strong charge transfer, the electronic configuration of BLi is similar to that of the atomic anion $B^-(^3P)$ interacting with the Li^+ ion.

Attachment of one excess electron to BLi ($^3\Pi$) to form a low spin anion leads to a bond stretching. The low spin state $^2\Sigma^+$ is the aground state of BLi^-, with a small doublet-quartet gap of −5.0 kcal/mol (CCSD(T)//MP2). Other values include −1.3 kcal/mol at B3LYP and −9.8 kcal/mol at MP2. The adiabatic electron affinity, that is calculated from the total energies of the neutral ($^3\Pi$) and the anion ($^2\Sigma^+$) is positive and equal to 0.57 eV at the CCSD(T)//MP2+ZPE level.

3.1.2. B_2Li

The high spin linear structure **III** ($^4\Sigma^-$) is the ground state at the B3LYP level. However, at the higher CCSD(T) level, the cyclic structure **II** (C_{2v}, $^2B_1$), in which Li-atom connects both B-atoms is the global minimum (Fig. 1). These two structures are however almost degenerate with a tiny energy gap of 0.2 kcal/mol. The next low-lying isomer is a high spin state (C_{2v}, $^4B_1$) being 6.0 kcal/mol higher in energy. The linear form **IV** in which Li-atom is located at center position of two B-atoms turns out to be very unstable.

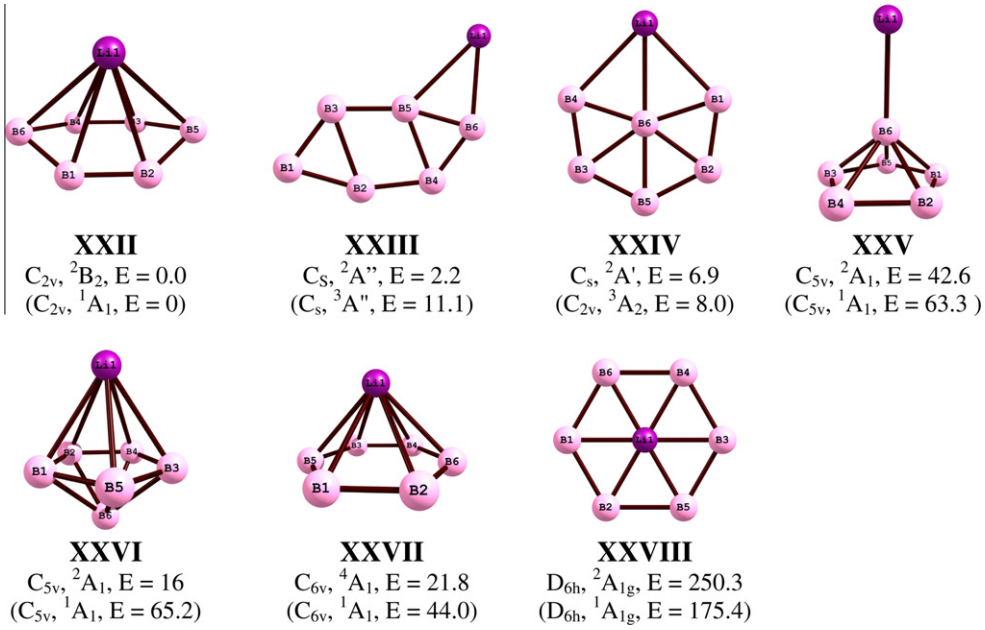

Fig. 4. Shape of the lowest-energy structures B_6Li and their anions. Relative energies (E) are given in kcal/mol for the neutrals (upper) and anions (lower).

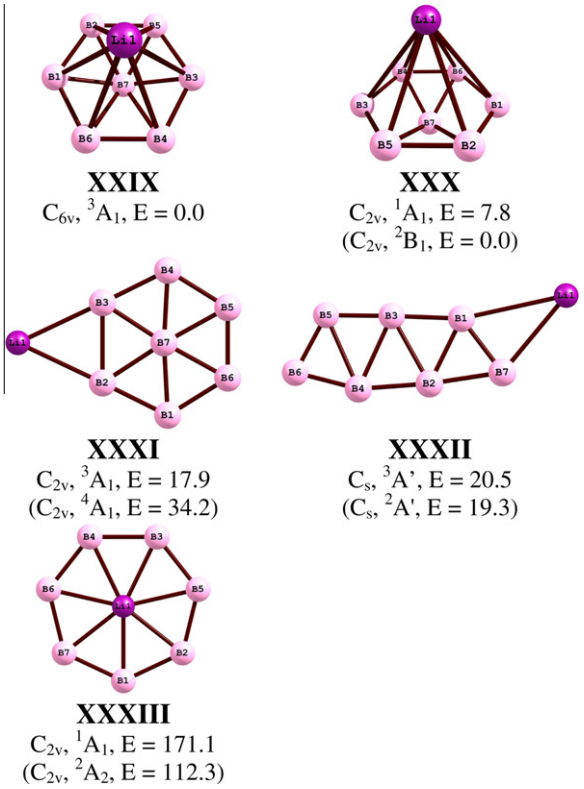

Fig. 5. Shape of the lowest-energy structures B_7Li and their anions. Relative energies (E) are given in kcal/mol for the neutrals (upper) and anions (lower).

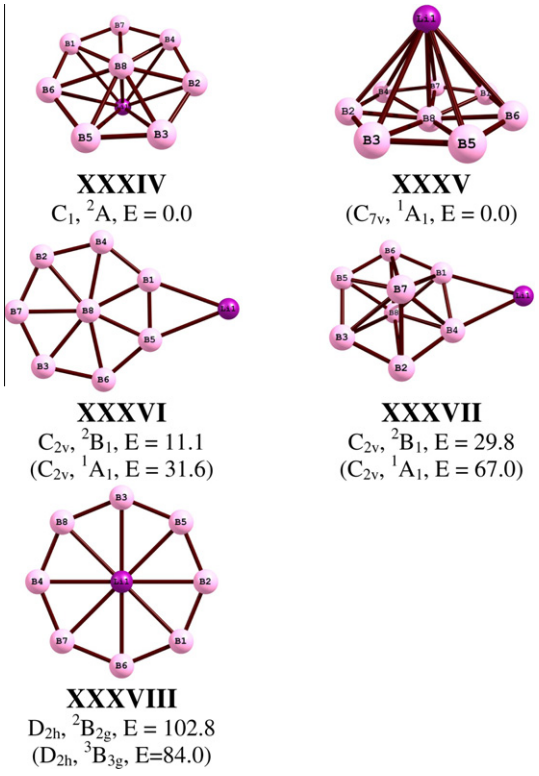

Fig. 6. Shape of the lowest-energy structures B_8Li and their anions. Relative energies (E) are given in kcal/mol for the neutrals (upper) and anions (lower).

Following attachment of one excess electron, the triplet state **II**$^-$ (C_{2v}, $^3B_1$) is the lowest-energy anionic form with a singlet–triplet gap of 11.7 kcal/mol (B3LYP). Another high spin (C_{2v}, $^3A_1$) is found to be the second lowest-lying isomer with an energy gap of 10.1 kcal/mol. The EA(B_2Li) calculated from total energies of **II** (C_{2v}, $^2B_1$) and **II**$^-$ (C_{2v}, $^3B_1$) is 1.00 eV (CCSD(T)). A small distortion of the C_{2v} neutral ($^2B_1$) from the C_{2v} anion ($^3B_1$) leads a negligible difference between both EA(B_2Li) and VDE(B_2Li^-) values (VDE = 0.98 eV).

3.1.3. B_3Li

The global minimum of these tetraatomic species is the trigonal pyramid **V** (C_{3v}, $^1A_1$) in which lithium is absorbed on the C_3 axis of the three-membered ring B_3 (D_{3h}). A planar structure **VI** (C_{2v}, $^1A_1$) in which Li connects with two B-atoms of B_3 ring is the next iso-

Table 1
Total atomization energies (TAE, kcal/mol), average binding energy (eV) and heats of formation (ΔH_f, kcal/mol) for the mixed clusters B_nLi (n = 1–8) calculated at the CCSD(T)/6-311+G(d)//B3LYP/6-311+G(d) level.

Structures	TAE (0K)	E_b (0K)	ΔH_f (0K)	ΔH_f (298K)
BLi **I** ($^3\Pi$)	24.1	0.52	148.7	149.5
B_2Li **II** ($^2B_1$)	114.6	1.66	193.3	194.3
B_3Li **V** ($^1A_1$)	252.3	2.74	190.7	191.9
B_4Li **IX** ($^2A'$)	334.8	2.9	243.3	244.7
B_5Li **XVI** ($^1A'$)	445.1	3.22	268.1	269.6
B_6Li **XXII** ($^2B_2$)	541.6	3.35	306.7	308.8
B_7Li **XXIX** ($^3A_1$)	673.9	3.65	309.5	310.7
B_8Li **XXXIV** (^2A)	805.1	3.88	313.4	315.6
BLi^- **I**$^-$ ($^2\sum^+$)	32.7	0.71	140.1	141.0
B_2Li^- **II**$^-$ ($^3B_1$)	137.0	1.98	170.9	172.0
B_3Li^- **V**$^-$ ($^2A'$)	265.1	2.87	177.9	179.3
B_4Li^- **X**$^-$ ($^1A_1$)	363.1	3.15	215.0	216.6
B_5Li^- **XVIII**$^-$ (^2A)	471.6	3.41	241.6	243.1
B_6Li^- **XXII**$^-$ ($^1A_1$)	597.0	3.7	251.3	252.9
B_7Li^- **XXX**$^-$ ($^2B_1$)	722.5	3.92	260.9	261.9
B_8Li^- **XXXV**$^-$ ($^1A_1$)	871.0	4.2	247.5	249.0

Table 2
Calculated adiabatic electron affinities (EA, eV) for all B_nLi structures considered at the CCSD(T)/6-311+G(d)+ZPE level.

Neutrals	Anions	B3LYP/6-311+G(d) geometries	MP2/6-311+G(d) geometries
BLi **I** ($^3\Pi$)	BLi^- **I**$^-$ ($^2\Sigma^+$)	0.37	0.57
B_2Li **II** ($^2B_1$)	B_2Li^- **II**$^-$ ($^3B_1$)	0.97	1.00
B_3Li **V** ($^1A_1$)	B_3Li^- **V**$^-$ ($^2A'$)	0.55	0.57
B_4Li **IX** ($^2A'$)	B_4Li^- **X**$^-$ ($^1A_1$)	1.23	1.27
B_5Li **XVI** ($^1A'$)	B_5Li^- **XVIII**$^-$ (^2A)	1.15	1.09
B_6Li **XXII** ($^2B_2$)	B_6Li^- **XXII**$^-$ ($^1A_1$)	2.40 (2.30 ± 0.10)[a]	
B_7Li **XXIX** ($^3A_1$)	B_7Li^- **XXX**$^-$ ($^2B_1$)	2.11	
B_8Li **XXXIV** (^2A)	B_8Li^- **XXXV**$^-$ ($^1A_1$)	2.86 (2.85 ± 0.10)[b]	

[a] Experimental value obtained from Ref. [24].
[b] Experimental value obtained from Ref. [25].

Table 3
Vertical detachment energies (VDEs, eV) of all B_nLi^- anions considered at the CCSD(T)/6-311+G(d) level.

Vertical neutrals	Anions	B3LYP/6-311+G(d) geometries	MP2/6-311+G(d) geometries
BLi **I** ($^3\Pi$)	BLi^- ($^2\Sigma^+$)	0.41	0.60
B_2Li **II** ($^2B_1$)	B_2Li^- ($^3B_1$)	0.97	0.98
B_3Li **V** ($^1A_1$)	B_3Li^- ($^2A_1$)	0.66	0.67
B_4Li **IX** ($^2B_2$)	B_4Li^- ($^1A_1$)	1.49	1.59
B_5Li **XVI** (^1A)	B_5Li^- (^2A)	1.51	1.56
B_6Li **XXII** ($^2B_2$)	B_6Li^- ($^1A_1$)	2.62 (2.60 ± 0.03)[a]	
B_7Li **XXIX** ($^3A_2$)	B_7Li^- ($^2B_1$)	2.27	
B_8Li **XXXIV** ($^2A_{1g}$)	B_8Li^- ($^1A_{1g}$)	3.08 (3.09 ± 0.05)[b]	

[a] Experimental value obtained from Ref. [24].
[b] Experimental value obtained from Ref. [25].

mer, being 7.1 kcal/mol higher in energy. Other isomers are located at >20 kcal/mol less stable than the global minimum.

For the anion B_3Li^-, a planar structure **VI**$^-$ (C_{2v}, $^2B_2$) is the lowest isomer at the B3LYP level. But at the higher CCSD(T) calculations, the structure **V**$^-$ (C_s, $^2A'$), that is distorted from high symmetry C_{3v} structure **V,** is a global minimum. **VI**$^-$ is the next isomer with ~4.0 kcal/mol higher in energy. The linear structures **VII**$^-$ and **VIII**$^-$ are much less stable being at least 33.7 kcal/mol above. The EA(B_3Li) and VDE(B_3Li^-) are equal to 0.55 eV and 0.66 eV, respectively (CCSD(T)), that are smaller than the corresponding values of the radical B_2Li (EA = 1.00 and VDE = 0.97 eV, see above). The low values of B_3Li are due to the high stability of the neutral **V**.

3.1.4. B_4Li

Various structures for B_4Li are explored using both B3LYP and MP2 levels (Fig. 2). The planar **IX** (C_s, $^2A'$) in which Li is connected with two B-atoms of the B_4 cycle (D_{2h}), is the global minimum. The following isomer is **X** (C_{2v}, $^2B_2$) being only 2.6 kcal/mol higher (B3LYP). It is remarkable to note that the three-dimensional structures such as **XI** (C_{2v}, $^2B_2$), **XII** (C_{2v}, $^2A_1$) and **XIII** (C_{4v}, $^2B_2$) have approximately the same energy content. At the MP2 level, both structures **XI** (C_{2v}, $^2B_2$) and **XII** (C_{2v}, $^2A_1$) are local minima, whereas **XIII** (C_{4v}, $^2B_2$) is a first-order saddle point having one imaginary frequency. The linear forms **XIV** and **XV** are much less stable as compared to other isomers.

Following addition of one excess electron to the SOMO of the doublet B_4Li, the closed shell form **X**$^-$ (C_{2v}, $^1A_1$) becomes the most stable form. Although the high spin **IX**$^-$ (C_s, $^3A'$) is the lowest in energy at the B3LYP level, it is now 6.1 kcal/mol less stable than **X**$^-$ at the CCSD(T) level. The EA(B_4Li) = 1.23 eV calculated from the anion **X**$^-$ and the neutral **IX** is significantly smaller than the VDE(B_4Li^-) value of 1.49 eV.

3.1.5. B_5Li

From B3LYP and MP2 calculations using the 6-311+G(d) basis set, Li et al. [21] found that the planar structure **XVI** (C_s, $^1A'$, Fig. 3) is the global minimum of B_5Li. Our calculated results concur with this and show that the alternative isomer **XVII** (C_1, $^1A'$) is 1.7 kcal/mol higher. At the coupled-cluster theory level, both structures become quasi-degenerate. The charge transfers from Li to the B_5 cycle in both structures are similar (q(Li) ~ 0.94 electron). The other isomers **XIX** and **XX** are much less stable than **XVI**.

For the anion B_5Li^-, **XVIII**$^-$ (C_1, ^2A), that is distorted from **XVII**$^-$, is predicted to be the global minimum. The planar structure **XXI**$^-$ (C_s, $^2A''$), that is derived from the neutral shape **XVI** (C_s, $^1A'$) is the next isomer, located at 2.4 kcal/mol above **XVIII**$^-$. The corresponding value EA(B_5Li) = 1.15 eV is quite smaller than the VDE(B_5Li^-) of 1.51 eV.

3.1.6. B_6Li

The three-dimensional structure **XXII** (C_{2v}, $^2B_2$) in which Li is absorbed on the B_6 cycle (D_{2h}) is the global minimum (Fig. 4). The planar **XXIII** (C_s, $^2A''$), in which Li binds to one B-atom of the B_6 (C_{2h}), is the second-lying isomer being only 2.2 kcal/mol above **XXII**. Another planar structure **XXIV** (C_s, $^2A'$) in which the Li impurity simply replaces one peripheral B of the six-membered ring B_7 (D_{6h}) is found to be next isomer located at 6.9 kcal/mol higher in energy than **XXII**. High symmetry structures displayed in Fig. 4 (**XXV**, **XXVI** and **XXVII**) are much less stable than the global minimum by at least 16 kcal/mol.

Formation of the anion ground state by attachment of one electron to the SOMO of **XXII** does not affect much its geometry, and consequently the global minimum of B_6Li^- keeps the pyramidal form **XXII**$^-$ (C_{2v}, $^1A_1$) [24]. The next lowest-lying isomer is the triplet **XXIV**$^-$ (C_{2v}, $^3A_2$) which is at 8.0 kcal/mol above, and this isomer was omitted in the previous report [24] The calculated VDE(B_6Li^-) and EA(B_6Li) results amount to 2.62 and 2.40 eV, respectively (CCSD(T)), that are in good agreement with the experimental values, namely 2.60 ± 0.03 eV for VDE and 2.3 ± 0.1 eV for EA [24].

3.1.7. B_7Li

Gong et al. [23] reported that a high spin (C_{6v}, $^3A_2$) is the global minimum of this size. Our calculations point out that the global minimum of B_7Li is having a different high spin state **XXIX** (C_{6v}, $^3A_1$), in which Li is attached on the C_6 axis of the B_7 (C_{6v}) cycle (Fig. 5). The low spin structure **XXX** (C_{2v}, $^1A_1$), that is a distortion from **XXIX,** is the second- lowest isomer with an energy gap of 7.8 kcal/mol.

Table 4
Calculated NBO populations of all global energy minima.

Structures	Li	B1	B2	B3	B4	B5	B6	B7	B8
BLi^- (**I**, $^2\Sigma^+$)	−0.09	−0.91							
BLi (**I**, $^3\Pi$)	0.74	−0.74							
B_2Li^- (**II**, $^3B_1$)	0.42	−0.71	−0.71						
B_2Li (**II**, $^2B_1$)	0.84	−0.42	−0.42						
B_3Li^- (**V**, $^2A'$)	0.49	−0.51	−0.51	−0.47					
B_3Li (**V**, $^1A_1$)	0.86	−0.29	−0.29	−0.29					
B_4Li^- (**X**, $^1A_1$)	0.82	−0.68	−0.23	−0.23	−0.68				
B_4Li (**IX**, $^2A'$)	0.94	0.14	−0.22	−0.29	−0.56				
B_5Li^- (**XVIII**, ^2A)	0.88	0.14	−0.11	−0.30	−0.04	−0.57			
B_5Li (**XVII**, $^1A'$)	0.94	−0.14	−0.04	−0.14	−0.04	−0.58			
B_6Li^- (**XXII**, $^1A_1$)	0.88	−0.25	−0.25	−0.25	−0.25	−0.44	−0.44		
B_6Li (**XXII**, $^2B_2$)	0.91	−0.13	−0.13	−0.13	−0.13	−0.20	−0.20		
B_7Li^- (**XXX**, $^2B_1$)	0.92	−0.39	−0.23	−0.39	−0.23	−0.23	−0.23	−0.21	
B_7Li (**XXIX**, $^3A_1$)	0.94	−0.13	−0.13	−0.13	−0.13	−0.13	−0.13	−0.19	
B_8Li^- (**XXXV**, $^1A_{1g}$)	0.93	−0.28	−0.28	−0.28	−0.28	−0.28	−0.28	−0.28	0.04
B_8Li (**XXXIV**, ^2A)	0.95	−0.10	−0.19	−0.03	−0.19	−0.10	−0.23	−0.03	−0.07

Table 5
NICS values for the lowest-lying isomers using GIAO//B3LYP/6-311+G(d)//B3LYP/6-311+G(d).

Structures	NICS			Structures	NICS		
	0	0.5	1.0		0	0.5	1.0
B_3Li **V** ($^1A_1$)	−62.7	−38.1	−11.9	B_3^- (D_{3h}, $^1A_1'$)	−74.3	−58.0	−27.7
B_4Li^- **X**$^-$ ($^1A_1$)	−40.2	−34.5	−21.4	B_4 (D_{2h}, ^1A_g)	−35.2	−24.0	8.0
B_5Li **XVI** ($^1A'$)	−12.8	−25.9	−14.8	B_5^- (C_{2v}, $^1A_1$)	−12.8	−25.9	−14.8
B_6Li^- **XXII**$^-$ ($^1A_1$)	5.3	12.3	16.8	B_6^{2-} (D_{2h}, ^1A_g)	−1.6	5.0	10.0
B_7Li **XXIX** ($^3A_1$)	−38.7	−34.1	−21.7	B_7^- (C_{6v}, $^3A_1$)	−11.6	−31.7	−18.3
B_8Li^- **XXXV**$^-$ ($^1A_{1g}$)	−9.5	−37.5	−24.8	B_8^{2-} (D_{7h}, $^1A_1'$)	−84.1	−26.9	−24.8

The anion B_7Li^- formed following attachment of one electron to the doubly degenerate SOMO of **XXIX** (C_{6v}, $^3A_1$) undergoes a strong Jahn–Teller distortion which results in **XXX**$^-$ (C_{2v}, $^2B_1$). The next isomer is the planar **XXXI**$^-$ (C_s, $^2A'$) being located at 19.3 kcal/mol above. Other structures are much less stable, being situated at >34 kcal/mol higher on the energy scale. The calculated EA(B_7Li) = 2.11 eV is slightly smaller than the corresponding value of VDE(B_7Li^-) = 2.27 eV.

3.1.8. B_8Li

Various geometrical features of B_8Li are investigated using both B3LYP and MP2 methods with 6-311+G(d) basis set. The 3D-structure **XXXIV** (C_s, ^2A) is the global minimum for this size (Fig. 6). The alterative structure **XXXVI,** in which Li connects with two peripheral B-atoms of the most stable B_8 (C_{2v}), is identified to be the second lowest-lying isomer, with a separation of 11.0 kcal/mol.

At the B3LYP/6-311+G(d) level, Alexandrova et al. [25] found that the global minimum of the anion B_8Li^- is a the low spin **XXXV**$^-$ (C_{7v}, $^1A_{1g}$) where the B-atom of the high symmetry B_8^{2-} (D_{7h}) is slightly out-of-plane distorted from the ideal seven-membered ring. Our CCSD(T) results obtained either using the B3LYP or MP2 optimized geometries concur with this prediction. The VDE(B_8Li^-) and EA(B_8Li) are calculated at 3.08 and 2.86 eV at the CCSD(T) level, respectively, that are in excellent agreement with the experimental values of 3.09 ± 0.05 eV for VDE and 2.85 ± 0.10 eV for ADE [25]. Thus, B_8Li possesses the highest EA value in the series B_nLi (n = 1–8) considered, due to the high stability of the high symmetry anion **XXXV**$^-$.

3.2. Chemical bonding and growth mechanism

Natural population analyses are performed using the B3LYP/6-311+G(d) densities. The charges and populations of the global minima are gathered in Table 4. For most structures, the positive charge is, as expected, mainly centered on Li, and the negative charge is distributed over the B-atoms. It is interesting to note that the geometries of the B_nLi global minima distort only slightly from the parent B_n. They can be considered either as complexes of B_n^- and Li^+ (for neutrals B_nLi) or as complexes of B_n^{2-} and Li^+ (for anions B_nLi^-).

This constitutes the main difference of the B_nLi clusters with respect to the boron oxides B_nO, in which the O-impurity significantly changes the B_n framework within B_nO as compared to the pure B_n counterparts by forming strong BO bond (cf. Ref. [18]). Doping a Li-atom distorts only slightly the B_n framework, and its results in an electrostatic interaction. As expected, the Li-atom prefers to form bridge with two or more B-atoms, except for the neutral B_5Li. In other words, the growth pattern of the doped B_nLi clusters is foreshadowed to that of the pure B_n clusters. The low-lying isomers for neutrals B_nLi predicted in Fig. 7 point out a motif to form the B_nLi clusters as followed: (i) lithium tends to form the complexes between Li^+ cation and host B_n^- and only distorts slightly their structure and (ii) there is competition between two motifs, including a planar feature of boron host and a tendency of maximum coordinate of Li-atom. The first is more dominant for small clusters B_nLi (n = 1–5). However, for larger clusters as $n \geqslant 6$, the later becomes more dominant. It can be observed that B_3Li (**V**) is remarkable stable specie in which the B_3 unit remains planar feature and Li-atom have maximum coordinate number of 3. Whereas the B_4Li prefers the planar structures **IX** and **X**, two structures **XVI** and **XVII** of B_5Li are almost degenerate. The larger systems B_nLi (n = 6–8) are three-dimensional structures.

3.3. Evaluation of aromaticity

Aromaticity of bare boron clusters in different charge states have been examined extensively in previous reports [5,9,10,16–19]. Recently, Alexandrova and co-workers [24,25] examined both

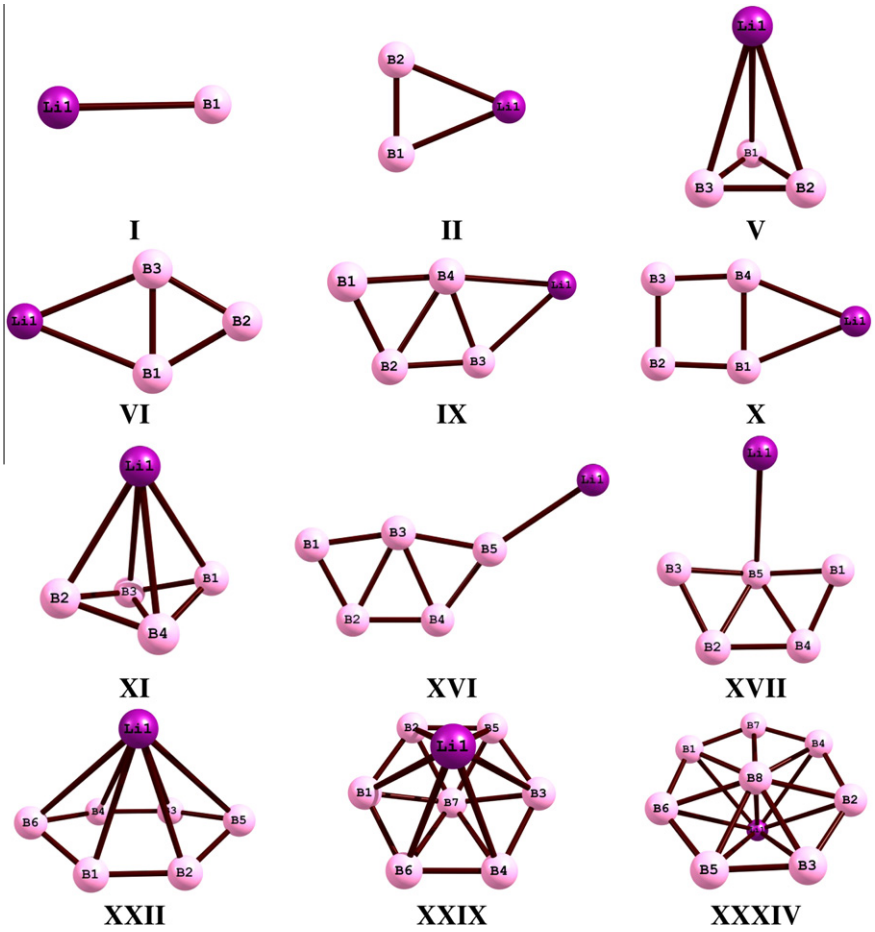

Fig. 7. Shape of the global minima of the neutrals B_nLi.

B_6Li^- and B_8Li^- anions and concluded that both cluster anions possess an aromaticity to be similar to their isoelectric species B_n^{2-} ($n = 6, 8$). A similar evaluation of MB_5 (M = Li, Na, K, Rb and Cs) and LiB_7 was carried out by Li and co-workers [21,23]. To probe further the aromatic character of the clusters, we perform for B_nLi an analysis similar to those of their parent boron clusters using the criteria such as nucleus-independent chemical shifts (NICS) and molecular orbital shapes.

Nucleus-independent chemical shifts (NICS) is based on magnetic shielding [54]. Negative NICS values characterize an aromatic character, whereas positive NICS values reveal an anti-aromaticity, and a non-aromaticity is characterized by NICS values close to zero. In this work, we calculate the NICS(0, 0), NICS(0, 0.5) and NICS(0, 1.0) for the B_nLi relative to the geometrical centers of the boron rings. The NICS values calculated for both B_n and B_nLi with closed shell electronic configurations are given in Table 5. It turns out that the NICS values for both series are quite similar to each other. The B_3Li (C_{3v}, $^1A_1$) has the highest NICS values in the B_nLi series, whereas the B_6Li^- (C_{2v}, $^1A_1$) reveals positive NICS values that suggest an anti-aromaticity. However, the NICS values obtained at the central positions of each of the two three-membered ring exhibit highly negative values, namely NICS(0) = −33.8 ppm; NICS(0.5) = −24.7 ppm; NICS(1.0) = −12.6 ppm, that support for the existence of a local aromaticity in B_6Li^-.

An analysis of clusters MOs is also carried out to probe further the electron distribution. Let us first present a comparison of the MOs picture between B_3^{2-} and B_3Li^-. As shown in Fig. 8, there is a negligible difference between the orbital features of both systems. The three orbitals HOMO-2, HOMO-3 and HOMO-4 are responsible for three BB bonds of the B_3 ring. The HOMO is a globally delocalized σ orbital, whereas HOMO-1 is a globally delocalized π orbital. In the same way as B_3^-, the neutral B_3Li possesses two delocalized σ electrons and two delocalized π electrons that make it doubly σ- and π-aromatic.

According to the NBO populations, a substantial charge transfer with q(Li) = 0.82 electron occurs in the ground state **X**$^-$ (C_{2v}, $^1A_1$), that leads the MOs shape and ordering of B_4Li^- to be similar to those of B_4^{2-} (Fig. 9). The B_4^{2-} dianion has been demonstrated to be a doubly (σ and π) aromatic system in previous reports [16]. Consequently, the B_4Li^- anion also behaves as a doubly (σ and π) aromatic system.

The MOs of B_5Li, B_6Li^-, B_7Li and B_8Li^- show similar pictures. A full set of MOs of these structures, and those of their corresponding pure boron clusters, are given in the Supporting Information (ESI). The presence of Li^+ only slightly perturbs the MOs of B_nLi as compared to the corresponding B_n. The canonical MOs of B_5Li **XVI** (C_s, $^1A'$) reveal that the HOMO-3 contains two globally delocalized π electrons, whereas the HOMO-1 is a globally bonding orbital. These globally delocalized orbitals constitute the origin for the doubly (π and σ) aromaticity of B_5Li.

It is worth noting that although the anion B_6Li^- **XXII**$^-$ (C_{2v}, $^1A_1$) is indicated by NICS as an anti-aromatic system, it is actually more stable than the other isomers. The HOMO-3 and HOMO-5 of B_6Li^- are global bonding orbitals, while the HOMO and HOMO-1 are partially σ and π bonding orbitals, respectively. As pointed out above by NICS values, this special distribution induces a local aromaticity for B_6Li^-, and that is in line with its stability.

Our evaluation for the aromaticity of B_7Li **XIX** (C_{6v}, $^3A_1$) and B_8Li^- **XXXV**$^-$(C_{7v}, $^1A_1$) agrees with the results obtained earlier by Gou et al. [23] and Alexandrova et al. [25]. B_7Li **XIX** (C_{6v}, $^3A_1$) is

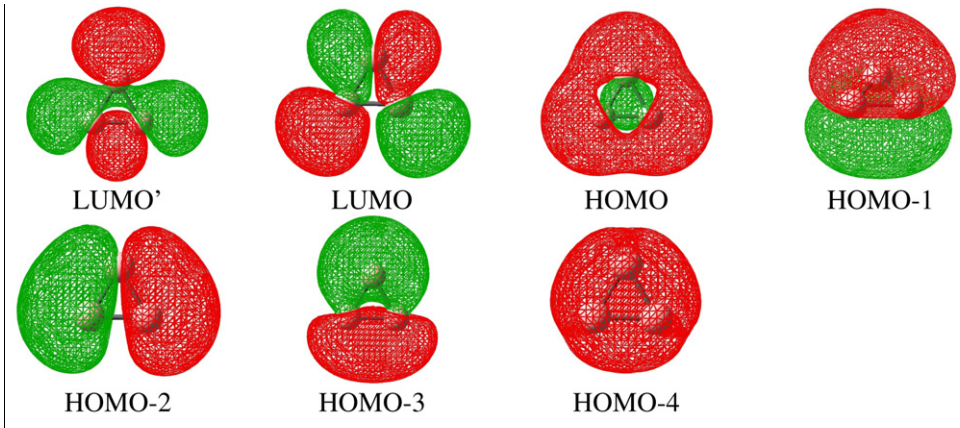

a. MO shapes of the B_3^- anion (D_{3h}, $^1A_1$')

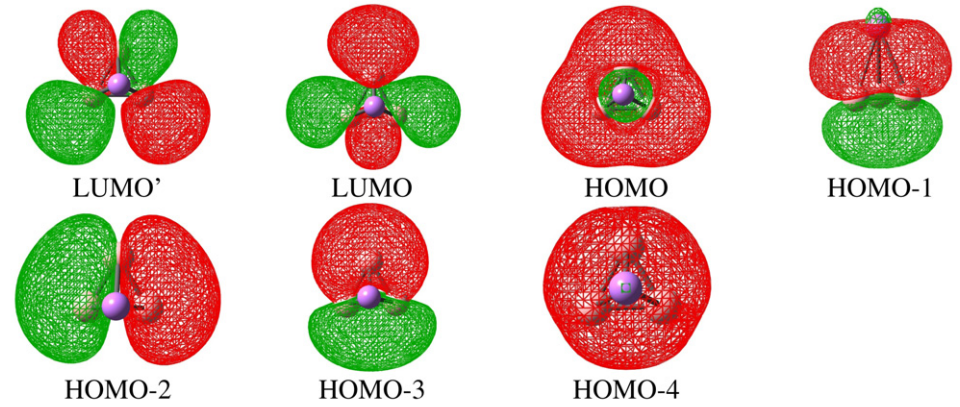

b. MO shapes of B_3Li (C_{3v}, $^1A_1$)

Fig. 8. MO shapes of (a) the B_3^- and (b) the B_3Li.

characterized with four delocalized σ electrons and four delocalized π electrons. Similar to the isoelectronic dianion B_8^{2-} (D_{7h}, $^1A'_1$), the B_8Li^- anion **XXXV**$^-$ (C_{7v}, $^1A_1$) contains six globally delocalized σ electrons and six globally delocalized π electrons, that render B_8Li^- a doubly (σ and π) aromatic.

3.4. Topology of electron localization function (ELF)

The topological analysis of the ELF is an efficient method to probe the chemical bonding and electron delocalization in compounds [55,56]. Isosurfaces of the total ELF plotted for the global minima of B_nLi are displayed in Fig. 10. The electron distribution of B_nLi are quite similar to those of the corresponding B_n shown in our recent reports [16,17]. The electron populations of the total ELF domains also confirm the presence of multi-center bonds, which are a typical feature in boron compounds. Overall, our results support for the view that the inherent features of the pure boron clusters such as strong electron delocalization, aromaticity and multi-center bonds remain the essential characteristics of the B_nLi clusters.

3.5. Energetic properties

The relative stability of clusters is further examined on the basis of the average binding energy (E_b), and the second difference in the total energy (Δ^2E) which are defined as follows:

$$E_b = [nE(B) + E(Li) - E(B_nLi)]/(n+1) \quad (1)$$

$$\Delta^2E(B_nLi) = E(B_{n-1}Li) + E(B_{n+1}Li) - 2E(B_nLi) \quad (2)$$

The E_b values of the bare and doped clusters in both neutral and anionic forms are compared in Fig. 11. The average binding energy tends to increase with the increasing B_n cluster size. Except for B_2Li and B_3Li, this energy term is actually decreased when Li is absorbed on boron clusters. A plot illustrating the dependence of the second difference with respect to the number of B-atoms (Fig. 12) emphasizes a remarkably high value for B_3Li. This provides an additional support for our above discussion on the closed shell configuration containing with 10 electrons of B_3Li.

In our recent reports [17,18], we have applied the resonance energy (RE) index and introduced the normalized resonance energy (NRE) as a new criterion to evaluate the stability of boron and boron oxide clusters. Our previous results demonstrated that the addition of O atoms to form electron-withdrawing BO substituents reduces the electron localization as compared to the parent boron clusters. Consequently, both the REs and NREs of the resulting boron oxides B_nO decrease relative to those of B_n. In a similar way, we define the REs of the neutrals B_nLi and anions B_nLi^- as expressed in Eqs. (3) and (4), respectively:

$$RE(B_nLi) = \Delta E(B_nLi \rightarrow nB + Li) - x\Delta E(B_2\left(^1\Sigma_g^+\right) \rightarrow 2B) - \Delta E(BLi(^3\Sigma^+) \rightarrow B + Li) \quad (3)$$

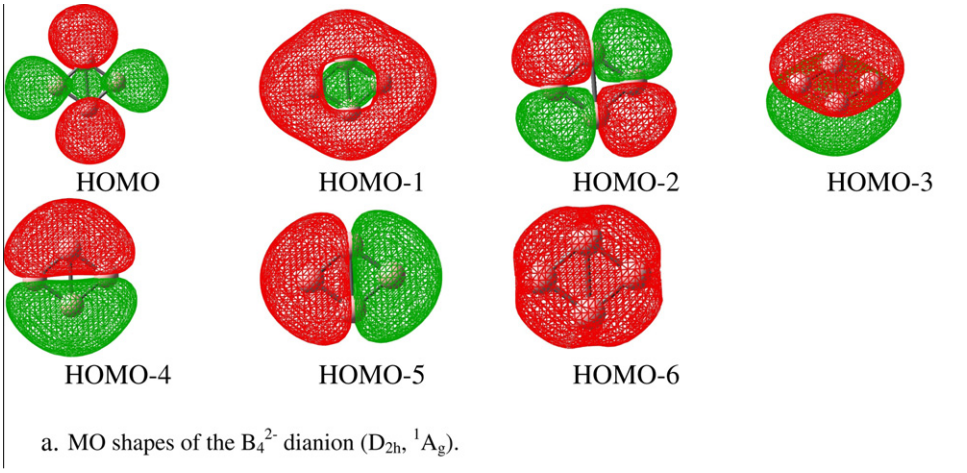

a. MO shapes of the B_4^{2-} dianion (D_{2h}, ^1A_g).

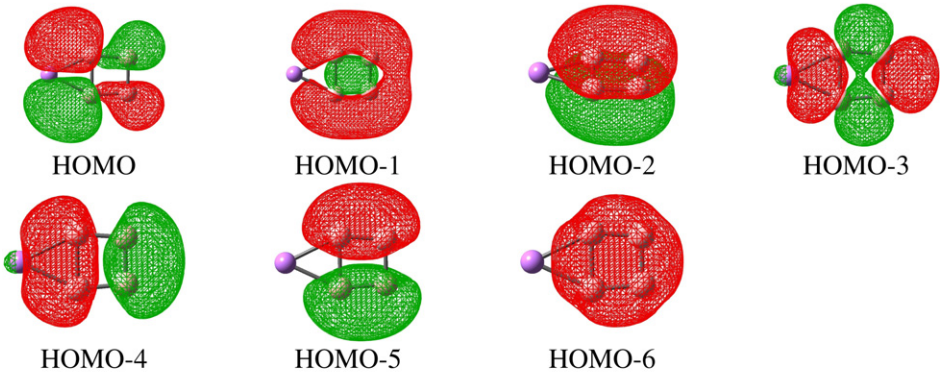

b. MO shape of the B_4Li^- anion (C_{2v}, $^1A_1$).

Fig. 9. MO shapes of (a) the B_4^{2-} and (b) the B_4Li^-.

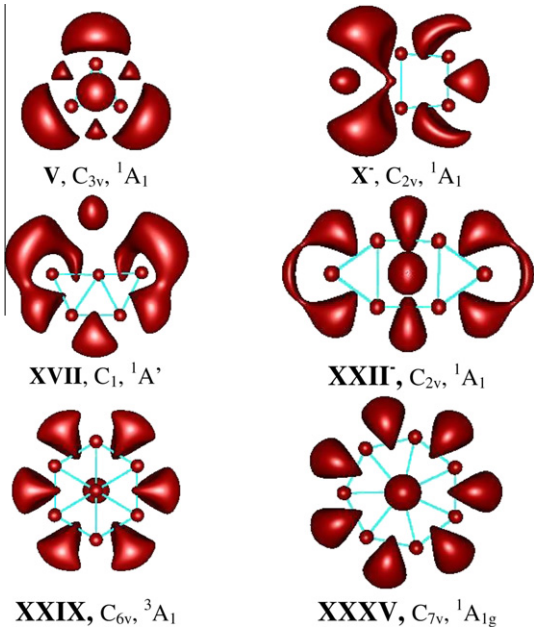

Fig. 10. ELF isosurfaces for the global minima in the range of 0.8–0.85.

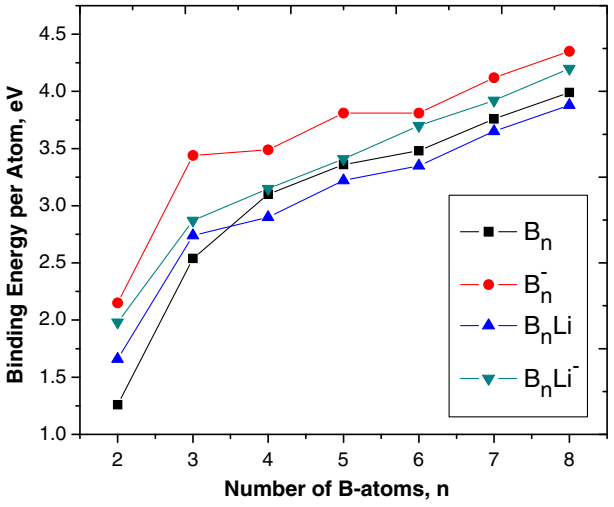

Fig. 11. Size dependence of the average energy per atom (E_b in eV) of B_n (black line), B_n^- (red line), B_nLi (blue line) and B_nLi^- (dark cyan line) clusters. (For interpretation of the references to colour in this figure legend, the reader is referred to the web version of this article.)

$$RE(B_nLi^-) = \Delta E(B_nLi^- \rightarrow nB + Li) - (x-1)\Delta E(B_2(^1\Sigma_g^+) \rightarrow 2B) - \Delta E(B_2^-(^4\Sigma_g^-) \rightarrow 2B + e) - \Delta E(Li(^2\Pi) \rightarrow B + Li) \quad (4)$$

in which the diatomic B_2 is the ground state $^1\Sigma_g^+$ and x is the number of the effective BB bonds available in B_n.

The normalized resonance energy (NRE) is simply defined as RE/(n + 1). To facilitate comparison, the REs and NREs of bare boron

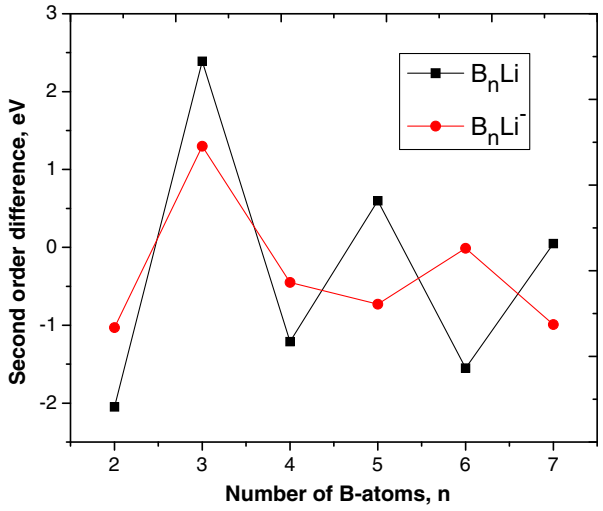

Fig. 12. Size dependence of the second-order energy difference B_nLi (black line) and B_nLi^- (red line) clusters. (For interpretation of the references to colour in this figure legend, the reader is referred to the web version of this article.)

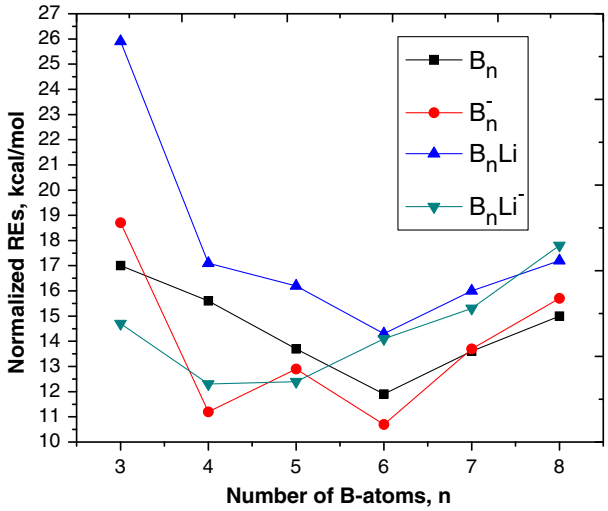

Fig. 14. Size dependence of the normalized resonance energies (NRE in kcal/mol) of B_n (black line), B_n^- (red line), B_nLi (blue line) and B_nLi^- (dark cyan line) clusters. (For interpretation of the references to colour in this figure legend, the reader is referred to the web version of this article.)

clusters in both neutral and anionic states are calculated from total atomic energies (TAEs) of the global minima using the same CCSD(T)/6-311+G(d)//B3LYP/6-311+G(d)+ZPE level. The values of x are taken from our previous reports [17,18], and the calculated REs and NREs values are given in the ESI. The dependence of REs and NREs values on number of B-atoms are schematically illustrated in Figs. 13 and 14. In contrast with the boron oxides in which BO groups are electron-withdrawing groups, both quantities REs and NREs of the Li-doped clusters are larger than those of the pure B_n clusters. Lithium is an electropositive element and its electron donation to the parent boron cluster is the main reason for these increases. In the same vein, the REs and NREs of the B_nLi neutrals have a tendency to be larger than those of the corresponding anions, except for B_8Li. Let us note that the anion B_8Li^- (C_{7v}, $^1A_1$) possesses a closed shell configuration and a high symmetry structure, as compared to the neutral B_8Li (C_1, ^2A), that results in larger RE and NRE values.

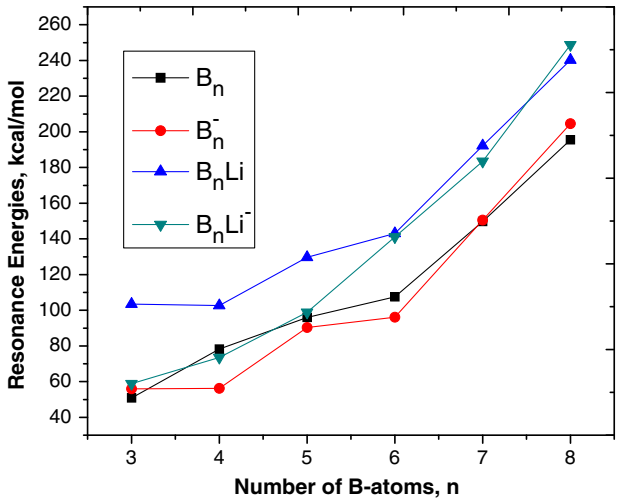

Fig. 13. Size dependence of the resonance energies (RE in kcal/mol) of B_n (black line), B_n^- (red line), B_nLi (blue line) and B_nLi^- (dark cyan line) clusters. (For interpretation of the references to colour in this figure legend, the reader is referred to the web version of this article.)

It is interesting to note that the NRE of the neutral B_3Li is very high as compared to other members. This result confirms our discussion above on the stability of the neutral B_3Li, which is also due to the inherent stability of the B_3^- anion [16].

3.5.1. Dissociation energies

To probe further the thermodynamic stability of the systems, we examine their dissociation energies. For the neutrals, the reaction energies for the following channels are considered:

$$B_nLi \rightarrow B_{n-1}Li + B$$
$$B_nLi \rightarrow B_n + Li$$

For the anionic clusters B_nLi^-, two dissociation channels are considered:

$$B_nLi^- \rightarrow B_n + Li^-$$
$$B_nLi^- \rightarrow B_n^- + Li$$

The calculated results for neutral clusters listed in Table 6 show that decomposition of the neutral B_nLi to give one Li-atom plus one fragment B_n is less endothermic than the others. For the anionic clusters, the energies of fragmented reactions giving one Li-atom plus one B_n^- fragment are consistently smaller as compared to those giving anion Li^- and specie B_n. These results are consistent with our predictions that the B_nLi clusters tend to be constructed by adsorbing one Li-atom on the backgrounds B_n or B_n^-.

Table 6
Dissociation enthalpies (kcal/mol) of the clusters B_nLi and B_nLi^- by using the CCSD(T)/6-311+G(d)//B3LYP/6-311+G(d) level.

Neutrals	$B_n + Li$	$B_{n-1}Li + B$	Anions	$B_n + Li^-$	$B_n^- + Li$
BLi **I** ($^3\Pi$)	23.3	172.8	BLi^- **I**$^-$ ($^2\sum^+$)	17.7	31.9
B_2Li **II** ($^2B_2$)	55.3	284.6	B_2Li^- **II**$^-$ ($^3B_1$)	63.5	36.9
B_3Li **V** ($^1A_1$)	75.4	329.4	B_3Li^- **V**$^-$ ($^2A'$)	73.9	25.5
B_4Li **IX** ($^2A'$)	47.2	327.0	B_4Li^- **X**$^-$ ($^1A_1$)	61.2	40.0
B_5Li **XVI** ($^1A'$)	56.4	379.8	B_5Li^- **XVIII**$^-$ (^2A)	68.8	31.2
B_6Li **XXII** ($^2B_2$)	57.6	404.7	B_6Li^- **XXII**$^-$ ($^1A_1$)	99.4	67.6
B_7Li **XXIX** ($^3A_1$)	65.3	443.9	B_7Li^- **XXX**$^-$ ($^2B_1$)	100.0	56.0
B_8Li **XXXIV** (^2A)	66.6	445.8	B_8Li^- **XXXV**$^-$ ($^1A_1$)	119.1	66.8

4. Conclusion

We present in this theoretical study a systematic investigation on a series of lithium doped boron clusters B_nLi ($n = 1–8$) in both neutral and anionic states. The energetically lowest-lying structures for these clusters are determined using both B3LYP and MP2 calculations. Addition of Li to B_n to form the B_nLi clusters distorts only slightly the geometries of the parent B_n clusters. Thermochemical properties for B_nLi clusters such as adiabatic electron affinities (EAs), vertical detachment energies (VDEs), total atomic energies (TAEs) and heats of formation (ΔH_f) at both 0 and 298 K are determined. Our calculated results show that there is a good agreement among various methods (B3LYP, MP2 and CCSD(T)). The EAs and VDEs values of B_6Li and B_8Li also agree well with the available experimental results.

Natural bonding orbital analysis points out that the chemical bonds in B_nLi have highly ionic character, in which the positive charges are mainly located on Li-atoms. Evaluation of the aromaticity for B_nLi based on the NICS values and molecular orbital shapes indicates a similarity in aromatic character between B_nLi and B_n^-. Most of the structures considered can be regarded as aromatic systems, that satisfy, among others, the classical Hückel $(4n + 2)$ rule for the planar systems.

The relative stabilities of structures are further evaluated by using the average binding energy (E_b), the second difference of the total energy ($\Delta^2 E$), resonance energy (RE) and normalized resonance energies (NRE). Both quantities REs and NREs of the Li-doped clusters are calculated to be larger than those of the pure B_n clusters. The structure B_3Li has a remarkably high stability within the B_nLi series.

Acknowledgments

M.T.N. is indebted to the K.U. Leuven Research Council for support (GOA and IDO programs). T.B.T. thanks the Arenberg Doctoral School for a scholarship. M.T.N. thanks the ICST of HoChiMinh City for supporting his stays in Vietnam.

Appendix A. Supplementary material

Tables contain the total energies and Cartesian coordinates for all optimized geometries. The shape of MOs of the dianions considered. Supplementary data associated with this article can be found, in the online version, at doi:10.1016/j.chemphys.2010.07.015.

References

[1] I. Boustani, Phys. Rev. B 55 (1997) 16426.
[2] A.K. Ray, I.A. Howard, K.M. Kanal, Phys. Rev. B 45 (1992) 14247.
[3] A. Ricca, C.W. Bauschlicher, Chem. Phys. 208 (1996) 233.
[4] J. Niu, B.K. Rao, B. Jena, J. Chem. Phys. 107 (1997) 132.
[5] A.N. Alexandrova, A.I. Boldyrev, H.J. Zhai, L.S. Wang, Coord. Chem. Rev. 250 (2006) 2811.
[6] J. Ma, Z. Li, K. Fan, M. Zhou, Chem. Phys. Lett. 372 (2003) 708.
[7] M.L. Drummond, V. Meunier, B.G. Sumpter, J. Phys. Chem. A 111 (2007) 6539.
[8] (a) Q.S. Li, Y. Zhao, W. Xu, N. Li, Int. J. Quant. Chem. 101 (2005) 219;
(b) Q.S. Li, L.F. Gong, Z.M. Gao, Chem. Phys. Lett. 390 (2004) 220.
[9] A.N. Alexandrova, A.I. Boldyrev, J. Chem. Theoret. Comput. 1 (2005) 566.
[10] H.J. Zhai, L.S. Wang, D.Y. Zubarev, A.I. Boldyrev, J. Phys. Chem. A 110 (2006) 1689. and references therein.
[11] (a) P.A. Hintz, S.A. Ruatta, S.L. Anderson, J. Chem. Phys. 92 (1990) 292;
(b) L. Hanley, S.L. Anderson, J. Chem. Phys. 89 (1988) 2848.
[12] (a) T.R. Burkholder, L. Andrews, J. Chem. Phys. 95 (1991) 8697;
(b) A.G. Maki, J.B. Burkholder, A. Sinha, C.J. Howard, J. Mol. Spectrosc. 130 (1988) 238.
[13] (a) G.J. Green, J.L. Gole, Chem. Phys. Lett. 69 (1980) 45;
(b) J.L. Gole, B. Ohllson, G. Green, Chem. Phys. 273 (2001) 59.
[14] B.M. Ruscic, L.A. Curtius, J. Berkowitz, J. Chem. Phys. 80 (1984) 3962.
[15] P.G. Wenthold, J.B. Kim, K.L. Jonas, W.C. Lineberger, J. Phys. Chem. A 101 (1997) 4472.
[16] M.T. Nguyen, M.H. Matus, V.T. Ngan, D.J. Grant, D.A. Dixon, J. Phys. Chem. A 113 (2009) 4895.
[17] T.B. Tai, D.J. Grant, M.T. Nguyen, D.A. Dixon, J. Phys. Chem. A 114 (2010) 994.
[18] T.B. Tai, M.T. Nguyen, D.A. Dixon, J. Phys. Chem. A 114 (2010) 2893.
[19] J.I. Aihara, H. Kanno, T. Ishida, J. Am. Chem. Soc. 127 (2005) 13324.
[20] B. Kiran, G. Gopakuma, M.T. Nguyen, A.K. Kandalam, P. Jena, Inorg. Chem. 48 (2009) 9965.
[21] Q.S. Li, Q. Jin, J. Phys. Chem. A 108 (2004) 855.
[22] Q.S. Li, Q. Jin, J. Phys. Chem. A 107 (2003) 7869.
[23] L.F. Gong, W.L. Guo, X.M. Wu, Q.S. Li, Chem. Phys. Lett. 429 (2006) 326.
[24] A.N. Alexandrova, A.I. Boldyrev, H.J. Zhai, L.S. Wang, J. Chem. Phys. 122 (2005) 054313.
[25] A.N. Alexandrova, H.J. Zhai, L.S. Wang, A.I. Boldyrev, Inorg. Chem. 43 (2004) 3552.
[26] (a) M.J.S. Dewar, C. deLlano, J. Am. Chem. Soc. 91 (1969) 789;
(b) C.G. Zhan, F. Zheng, D.A. Dixon, J. Am. Chem. Soc. 124 (2002) 14795.
[27] M.J. Frisch et al., Gaussian 03, Revision C.01, Gaussian, Inc., Wallingford, CT, 2004 (full reference is given in the ESI).
[28] H.-J. Werner et al., MOLPRO, version 2008.1, A Package of Ab Initio Programs (full reference is given in the ESI).
[29] R.G. Parr, W. Yang, Density-Functional Theory of Atoms and Molecules, Oxford University Press, Oxford, 1989.
[30] A.D. Becke, J. Chem. Phys. 98 (1993) 5648.
[31] J.P. Perdew, J.A. Chevary, S.H. Vosko, K.A. Jackson, M.R. Pederson, D.J. Singh, C. Fiolhais, Phys. Rev. B 46 (1992) 6671.
[32] J.A. Pople, J.S. Binkley, R. Seeger, Int. J. Quant. Chem. Symp. 10 (1976) 1.
[33] T. Clark, J. Chandrasekhar, G.W. Spitznagel, P.V.R. Schleyer, J. Comput. Chem. 4 (1983) 294.
[34] A.D. McLean, G.S. Chandler, J. Chem. Phys. 72 (1980) 5639.
[35] M.J. Frisch, J.A. Pople, J.S. Binkley, J. Chem. Phys. 80 (1984) 3265.
[36] R. Krishnan, J.S. Binkley, R. Seeger, J.A. Pople, J. Chem. Phys. 72 (1980) 650.
[37] J. Cizek, Adv. Chem. Phys. 14 (1969) 35.
[38] P.J. Knowles, C. Hampel, H.J. Werner, J. Chem. Phys. 99 (1993) 5219.
[39] K. Raghavachari, G.W. Trucks, J.A. Pople, M. Head-Gordon, Chem. Phys. Lett. 1 (1984) 57.
[40] A. Karton, J.M.L. Martin, J. Phys. Chem. A 111 (2007) 5936.
[41] M.W. Chase Jr., NIST-JANAF Themochemical Tables, fourth ed., J. Phys. Chem. Ref. Data, Monograph 9, 1998, p. 1951.
[42] D. Feller, K.A. Peterson, D.A. Dixon, J. Chem. Phys. 129 (2008) 204105.
[43] L.A. Curtiss, K. Raghavachari, P.C. Redfern, J.A. Pople, J. Chem. Phys. 106 (1997) 1063.
[44] A.E. Reed, L.A. Curtiss, F. Weinhold, Chem. Rev. 88 (1988) 899.
[45] J.P. Perdew, J.A. Chevary, S.H. Vosko, K.A. Jackson, M.R. Pederson, D.J. Singh, C. Fiolhais, Phys. Rev. B 46 (1992) 6671.
[46] T. Clark, J. Chandrasekhar, G.W. Spitznagel, P.v.R. Schleyer, J. Comput. Chem. 4 (1983) 294.
[47] A. Becke, K. Edgecombe, J. Chem. Phys. 92 (1990) 5397.
[48] (a) B. Silvi, A. Savin, Nature 371 (1994) 683;
(b) A. Savin, A. Becke, D. Flad, R. Nesper, H. Preuss, H.V. Schnering, Angew. Chem. Int. Ed. 30 (1991) 40.
[49] (a) S. Noury, X. Krokidis, F. Fuster, B. Silvi, TOPMOD Package, Universite Pierre et Marie Curie, Paris, 1997;
(b) S. Noury, X. Krokidis, F. Fuster, B. Silvi, Comput. Chem. 23 (1999) 597. Oxford.
[50] L. Laaksonen, J. Mol. Graph. 10 (1992) 33.
[51] Y. Li, D. Wu, Z.R. Li, C.C. Sun, J. Comput. Chem. 28 (2007) 1677.
[52] K.A. Nguyen, K. Lammertsma, J. Phys. Chem. A 102 (1998) 1608.
[53] A.I. Boldyrev, J. Simons, P.v.R. Schleyer, J. Chem. Phys. 99 (1993) 8793.
[54] (a) M. Hofmann, P.v.R. Schleyer, Inorg. Chem. 38 (1999) 652;
(b) M. Unverzagt, H.J. Winkler, M. Brock, M. Hofmann, P.v.R. Schleyer, W. Massa, A. Berndt, Angew. Chem. Int. Ed. Engl. 36 (1997) 853.
[55] B. Silvi, J. Mol. Struct. 614 (2002) 3.
[56] J. Poater, M. Duran, M. Sola, B. Silvi, Chem. Rev. 105 (2005) 3911.